MISR Prelaunch Instrument Calibration and Characterization Results

Carol J. Bruegge, Valerie G. Duval, Nadine L. Chrien, Robert P. Korechoff, Barbara J. Gaitley, and Eric B. Hochberg

Abstract— Each of the nine cameras that compose the Multi-angle Imaging SpectroRadiometer (MISR) has been rigorously tested, characterized, and calibrated. Requirements on these tests include a 3% (1σ) radiometric calibration requirement, spectral response function determination of both the in- and out-of-band regions, and distortion mapping. The latter test determines the relative look-angle to the ground corresponding to each focal plane detector element. This is established to within one-tenth of the instantaneous field-of-view. Most of the performance testing was done on the cameras as they completed assembly. This was done to take advantage of the serial delivery of the hardware, minimize the required size of the thermal-vacuum facilities, and allow testing to occur early in the schedule allocated for the hardware build. This proved to be an effective strategy, as each of the test objectives was met. Additional testing as an integrated instrument included verification of the data packetization, camera pointing, and clearances of the fields-of-view. Results of these studies have shown that the MISR cameras are of high quality and will meet the needs of the MISR science community. Highly accurate calibration data are on-hand and available for conversion of camera output to radiances.

Index Terms— Calibration, image sensors, testing.

I. INTRODUCTION

THE MULTI-ANGLE Imaging SpectroRadiometer (MISR) instrument, to be launched in 1998 as one of five instruments on the first Earth Observing System platform (EOS-AMI), has been designed and built by the Jet Propulsion Laboratory (JPL), California Institute of Technology, Pasadena. Details of the instrument design and scientific objectives are given elsewhere in this IEEE TRANSACTIONS ON GEOSCIENCE AND REMOTE SENSING EOS special issue [1]–[4]. The instrument consists of nine independent cameras, each with a unique view angle to earth. Each camera makes use of four charge-coupled device (CCD) line arrays, filtered to spectral bands that are measured to be 446, 558, 672, and 866 nm (as determined from a solar weighted, in-band moments analysis). These are termed, respectively, Bands 1–4 or Blue, Green, Red, and Near-Infrared (NIR). Each camera additionally consists of its own individual lens, camera head electronics, and analog-to-digital converter.

There exist 1504 active elements per CCD line array, each of which produces a 14-bit digital number (DN) output referred to as a data pixel. In addition to DN from active detector elements, there are also output samples called "overclock pixels." These latter signal-chain samples are created by sampling the CCD output after each of the 1504 active pixel wells has been clocked out for a given line read. Knowledge of this offset is essential, as it is the baseline upon which the light-sensitive signal sits. Although this baseline is dynamic, having a time constant of about 25 line samples, it is easily determined for each line of data. The dynamic baseline is a design feature that prevents loss of data should the nature of the dark current change on-orbit, for example, due to radiation damage. For MISR, a channel refers to the signal chain that produces DN from a given CCD line array. MISR has 36 data channels.

Planning for the calibration and characterization of the instrument evolved in parallel with the instrument design itself. Peer support was provided through semiannual meetings of the EOS calibration working group, consisting of representatives from the instrument development teams, universities, and the National Standards Laboratory. Peer reviews of each of the proposed instrument test programs were held. Equally important were the round-robin experiments. One experiment of this nature involved transporting several travelling radiometer standards, maintained by a variety of institutions, to the JPL calibration laboratory [5]. These were used along side the MISR standards, to cross compare the measured output of the integrating sphere. In this way, the radiometric scale defined for MISR was verified. A second round-robin experiment circulated diffuse-reflectance targets among EOS-affiliated institutions. These were measured for bidirectional reflectance factor (BRF), and a comparison of results was made [6]. Validation of these measurements is important, in that they are used for the on-orbit calibration of MISR using both the On-Board Calibrator (OBC) and vicarious calibration [7] methodologies.

One of the first activities of the calibration working group was to determine common nomenclature and terminologies [8]. As defined by this committee, calibration came to be known as an activity that produces a data set that describes some instrument property and whose data are to be used by the standard product processing algorithms. These standard products include the radiance product (termed the Level 1 product) and the retrieved geophysical parameter products (Level 2 products). Characterization is the acquisition of all

other quantitative values, used to describe some aspect of instrument performance, but not needed for standard product generation. Verification is the determination of a pass or fail condition, with respect to a design specification. Finally, validation is the process of certifying the accuracy of a retrieved geophysical parameter through an independent measurement.

During the MISR construction and performance evaluation process, data were collected both from the individual cameras (removed from and operated independently of the other MISR subsystems) and as an assembled instrument. As a camera includes the lens, filter, detector, and analog-to-digital electronics, this hardware uniquely determines the sensitivity to an incoming photon for those data channels. For this reason, it is sufficient to conduct calibration tests on a camera in isolation of the other subsystems. The instrument system, conversely, is responsible for pixel averaging, digital number compression via square-root encoding, and data packetization. Instrument level tests must therefore verify these instrument functions.

In making use of these test data, the MISR calibration team must keep track of differences in output pixel order between the camera and instrument data output formats. As the output pixel order for camera data is the CCD clocking order, this differs from the pixel ordering defined for the on-orbit data products. The latter are archived in a west-to-east sampling order. It is noted that not all cameras have the same orientation onto the MISR optical bench. Specifically, camera data acquired from the nadir and aft cameras are reversed in pixel order prior to archiving.

The key calibration activities conducted prelaunch, in support of MISR, are discussed in the sections to follow. The MISR calibration data are delivered to the standard processing center in the form of an Hierarchical Data Format (HDF) file. This data file is called the Ancillary Radiometric Product (ARP) and is described in [9]. Other references that provide additional information on the MISR calibration program are given in [10]–[15].

II. Spectral Calibration

The measured spectral response profiles are used in the production of the Level 1 radiance product and to interpret science products. Analysis of the spectral response functions can lead to descriptor parameters for the instrument, such as center wavelength and bandwidth. These are a mathematical convenience, useful in defining specifications, in comparing pixel-to-pixel or camera-to-camera response differences, or in assigning a wavelength at which a geophysical parameter (e.g., surface reflectance or atmospheric transmittance) is reported.

In computing the center wavelength and bandwidth of the spectral response functions, the moments analysis is used. This approach often provides the most accurate approximation to the more exact integral [16]. We additionally make the assumption that many top-of-atmosphere (TOA) radiance measurements will have the same relative spectral distribution as the solar spectrum. In our moments analysis, therefore, we weight the camera response function by the exo-atmospheric solar irradiance. The as-built MISR wavelengths that are

quoted are those descriptive of the in-band response region, weighted by the solar spectrum

$$
\begin{aligned}
\lambda_{m,\,\text{solar}}^{\text{std, in-band}} \\
&= \left(\int_{\text{in-band}} E_{o\lambda} S_\lambda \lambda \, d\lambda \right) \Big/ \left(\int_{\text{in-band}} E_{o\lambda} S_\lambda \, d\lambda \right) \\
\sigma^2 &= \left(\int_{\text{in-band}} E_{o\lambda} S_\lambda \lambda^2 \, d\lambda \Big/ \int_{\text{in-band}} E_{o\lambda} S_\lambda \, d\lambda \right) \\
&\quad \cdot \left[-(\lambda_{m,\,\text{solar}}^{\text{std,in-band}})^2 \right] \\
\lambda_{u,\,1} &= \lambda_{m,\,\text{solar}}^{\text{std, in-band}} \pm \left(\sqrt{3} \cdot \sigma \right) \\
\Delta \lambda_{m,\,\text{solar}}^{\text{std, in-band}} &= 2\sqrt{3} \cdot \sigma.
\end{aligned}
\tag{1}
$$

Here the symbol "std" refers to an analysis done using the standardized spectral response function S_λ, m refers to the moments analysis, and u and l refer to the equivalent square band upper and lower wavelength limits, respectively.

The exo-atmospheric solar irradiance $E_{0\lambda}$ model used by MISR is one recommended by the EOS calibration panel. Although the data are published by the World Climate Research Programme [17], they are included for reference in the MISR ARP. Values are reported at 1 astronomical unit (AU).

The calibration reports also provide a Gaussian representation of the MISR in-band regions. This is because the MISR filters were designed to be Gaussian in shape, allowing a polarization insensitive camera design when used in conjunction with a Lyot depolarizer [5]. These Gaussian parameters are additionally reported in the ARP and are thus available to the scientific community.

Spectral calibration of the MISR cameras was performed at the camera level (prior to assembly onto the instrument optical bench) under thermal vacuum conditions. Simply stated, the spectral response is determined as the ratio of the camera output DN_λ to the relative spectral output distribution of the incident source. A single grating monochromator is used as the source, with a xenon lamp and adjustable exit slit. The exit aperture is fitted with an integrating sphere to improve spectral uniformity of the emitted light. This modification to the original test configuration was crucial, in that only in doing so were the test results consistent and independent of setup alignment. Another improvement allowed the 0.5-nm spectral accuracy requirement to be met. Originally, mercury lamps were used for the monochromator wavelength calibration. This source is known to have emission lines broadened by collisions. The improvement was in the utilization of low-pressure penlight discharge lamps containing Neon (for the 530–648-nm region) or Argon (for the 694–864-nm region). The narrow emission lines from these sources are known to within ±0.1-nm uncertainty and, thus, provide a reference standard of high accuracy.

During the experiment, the monochromator output is first observed by unfiltered laboratory detector standards. The standards are known to have a uniform response to photons, independent of wavelength, and thus provide a spectral normalization function to obtain the effective camera response to a spectrally neutral source. When illuminating a camera, the sphere exit aperture simultaneously illuminates a camera
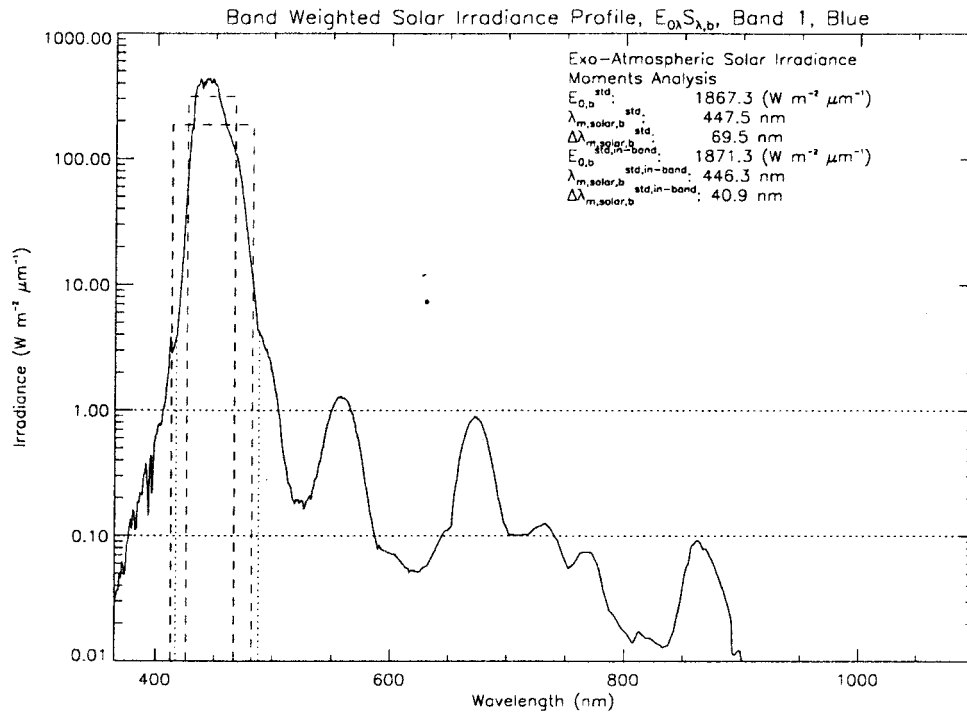
Fig. 1.　Standardized spectral response function for the Blue Band.

"zone" of about 50 cross-track pixels at all bands. A scan mirror between the monochromator sphere and camera is used to deviate the output, such that coverage is obtained for multiple camera zones sampling the field-of-view. At each zone, the monochromator is scanned between 400–900 nm. Following this, the next zone is illuminated and the monochromator scan repeated. Due to the time required to obtain test data, only three equally spaced zones are tested for both the in- and out-of-band response characterization (about 10% of the array). For an in-band scan, data are acquired at 2.6-nm spectral resolution and 0.5-nm sampling; for the out-of-band scan, the resolution is 19.6 nm and sampling is every 10 nm.

As both in- and out-of-band runs are used to characterize the cameras, these must be combined into one profile. The in-band runs have the advantage of high spectral resolution, which is needed to evaluate an effective band center and width. However, during these in-band runs, there is insufficient response to characterize the out-of-band region. For the out-of-band scans, the monochromator exit slit is opened, allowing greater illumination, as needed for detection of the response in this region. Care is taken to preserve the relative scale when merging the two data sets. This is accomplished by using the system radiometric model, described in a later section.

The last step performed to create a final response curve is to extend the region to all wavelengths for which the MISR cameras have sensitivity. The radiometric/spectral model data are thus used between 365 and 400 nm and 900 and 1100 nm. Additionally, the peak of the composite array is assigned an absolute transmittance from the model, with the measured relative response being preserved between 400 and 900 nm.

Once the spectral response functions were measured for each channel, the results were summarized by averaging all spectra for a given band. These averages are referred to as the standardized spectral response profiles. Variations in measured in-band center wavelength across the array were less than 2 nm from the value determined from the standardized response profile [18]. The standardized response profiles are depicted in Figs. 1–4 for the four MISR bands, respectively. In these figures, the square-band equivalent response functions are depicted with dashed lines. This is done for the equivalent in-band and total-band regions. The dashed lines represent the delineation of the region used in the in-band moments analysis. These transition points are at 1% of the peak response. The in-band center wavelengths, as shown by the labels, are 446.3, 557.5, 671.8, and 866.5 nm, with widths of 40.9, 27.2, 20.4, and 38.6 nm.

The integrated out-of-band response is found to vary with spectral channel, being greatest in the NIR channel. The average response for the four bands was determined to be 1, 2–3 (depending on the camera), 2, and 0.8–2%. As the out-of-band specification was written so as to verify a 1% integrated out-of-band response, it is evident that some channels did not meet this requirement. For this reason, the standardized spectral response functions are available to provide an out-of-band correction to the data for certain Level 2 products (most notably, the aerosol and land-surface products, but not the cloud products). Analysis has shown that the four MISR bands can be used to measure the spectral content of the scene and provide an accurate out-of-band correction to the measured radiances [19].

III. RADIOMETRIC CALIBRATION

A. Integration Time Selection

Although the integration times for each MISR channel are individually selectable, these camera parameters have been
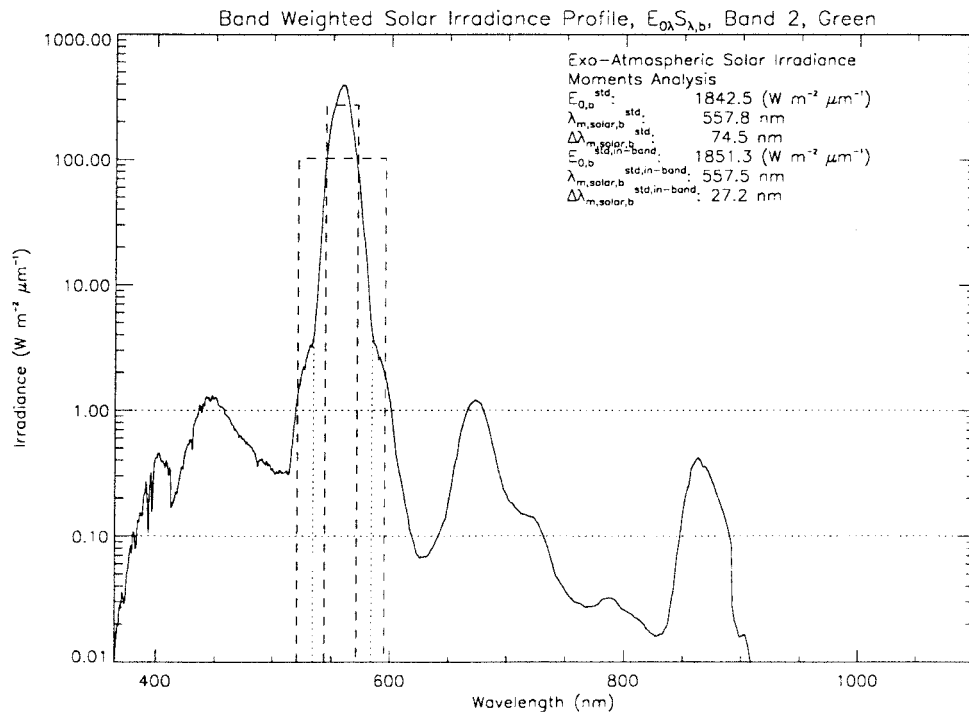
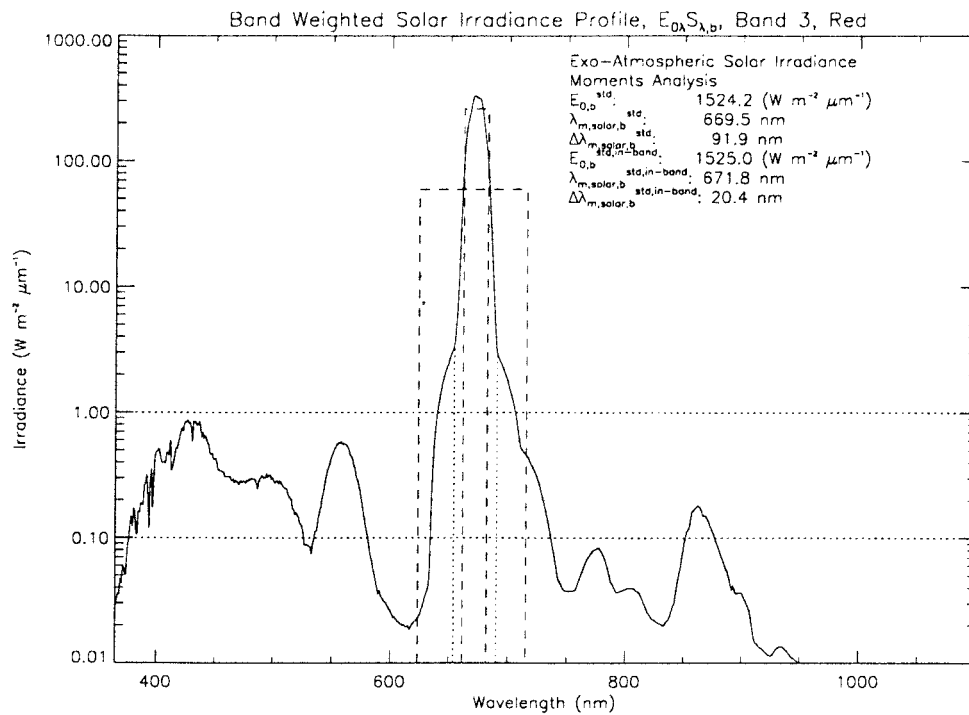Fig. 2. Standardized spectral response function for the Green Band.

Fig. 3. Standardized spectral response function for the Red Band.

established during preflight testing. This is required in that radiometric response is a function of integration time. The integration time is set such that the SNR specifications are just met at the edge-of-field, where the system transmittance is smallest. This allows the greatest margin between detector saturation and scene radiance. On-orbit integration times will only be changed if severe degradation is observed. The radiometric calibration will be reestablished from on-orbit procedures, should this occur.

B. Response Determination

During radiometric calibration, the relationship between an incident radiance field and camera digital output is established.
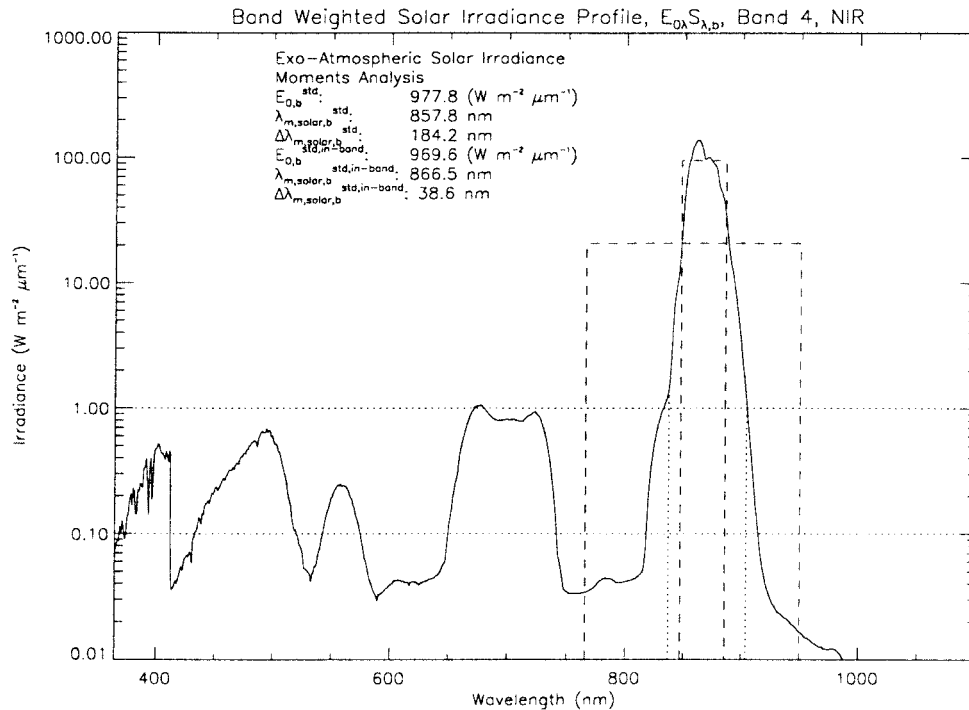
Fig. 4. Standardized spectral response function for the NIR Band.

The illumination is achieved using an "ideal" target that emits or reflects unpolarized light, is spatially and angularly uniform, and lacks spectral features, such as absorption lines. For preflight calibration, MISR made use of a large integrating sphere to provide this source. Through regression of the sphere exitance against the camera output, the radiometric gain coefficients are determined and the instrument is thereby radiometrically calibrated.

The sphere output is placed on a radiometric scale by measurements made with detector standards. (MISR is unique among the EOS-AM1 instruments, in that the radiometric scale is determined preflight and on-orbit using detector standards.) In order to achieve the highest radiometric accuracy, two types of laboratory detector standards are used. A QED-200 (made of United Detector Technology inversion layer diodes) is used to measure sphere output for the Blue and Green MISR spectral bands, Bands 1 and 2; and a QED-150 (made of Hamamatsu p-on-n photodiodes) is used for the Red and NIR channels, Bands 3 and 4. Each detector is nearly 100% in internal quantum efficiency for the wavelength regions at which they are operated. Each is made of three silicon photodiodes, mounted in a light-trap configuration so as to collect the light reflected at each air/detector interface. These standards are used with filters of the same spectral bandpass design as the flight cameras and with a known field-of-view established by use of a precision aperture tube. Traceability to Système International (SI) units is established through the measurement protocols of current, apertures, and aperture distances. JPL maintains working standards of voltage, resistance, and length that are traceable to the National Institute of Standards and Technology (NIST) or other international standards that are recognized by NIST. The filter transmittance for the standards

are measured by a dual-beam spectrometer, also requiring certification. The quantum efficiency and reflectance losses of the standards are assumed to be unity and zero, respectively, per design of the trap devices.

As these standards are photoconductive devices, they produce a current in response to incident photons. This relationship can be expressed by

$$i_\lambda = R_\lambda^{\text{diode}} q N_\lambda. \tag{2}$$

Here R_λ^{diode} is the photodiode spectral response as a function of wavelength λ and determined as the product of the detector quantum efficiency, filter transmittance, and front surface reflections. Other parameters are i, the device output current, q, the electron charge, and N_λ, the photon rate. Next utilized is the energy per photon expression $E_\lambda = hc/\lambda$, with h being Planck's constant and c being the speed of light. The photon rate is found as the ratio of incident flux Φ_λ to photon energy, where $\Phi_\lambda = L_\lambda A\Omega$, L_λ is the incident spectral radiance (identical for the diode and camera) in units of W m^{-2}sr^{-1} μm^{-1} and $A\Omega$ is the photodiode étendue (area times field-of-view product). From these, it is determined that the spectral radiance measured by the photodiode is

$$L_b = \frac{i\,1.2395\,\text{W}\,\mu\text{m}\,\text{Amps}^{-1}}{A\Omega \int_{0.2}^{1.2} N_\lambda R_\lambda^{\text{diode}} \lambda\, d\lambda}. \tag{3}$$

The subscript b is used to denote the wavelength at which this spectral radiance is reported. It is the photodiode center wavelength, as determined by a moments analysis of the diode spectral response function. Since there are four laboratory standard configurations, one corresponding to each of the four MISR bands, there are thus four measures of camera-incident
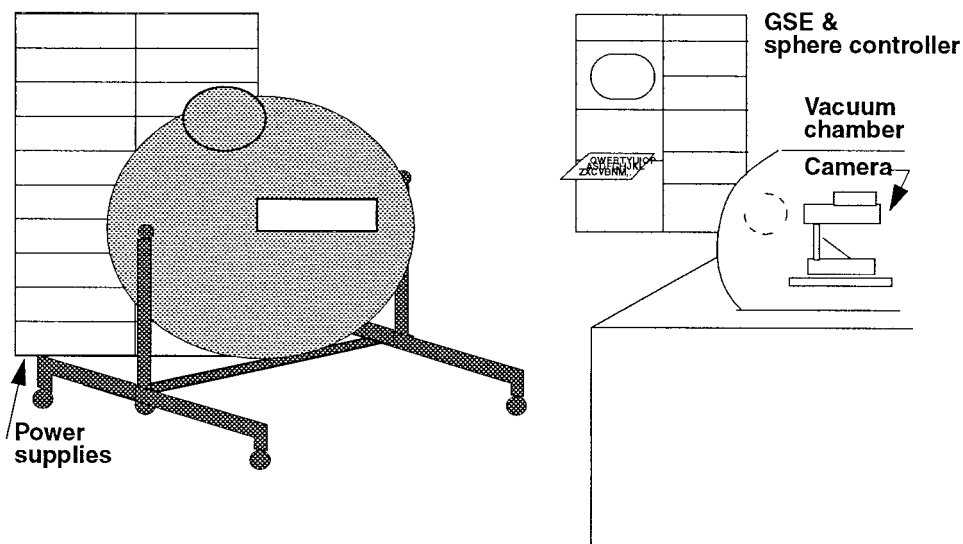
Fig. 5. Radiometric calibration layout.

radiance L_b. The denominator in (3) contains an estimate of the normalized source spectral output distribution N_λ. For preflight calibration, we estimate N_λ from the spectral Planck blackbody function at a bulb color temperature of 3100 K, normalized by the value of this function at wavelength b. (The temperature value is provided by the sphere vendor). Only a rough estimate of this distribution is needed, as its amplitude is scaled by the laboratory standard reading and the out-of-band response of the standard is quite low. The limits of integration are those of the photodiode response in μm.

In the above, the derived spectral radiance L_b is a property only of the incident field, independent of the photodiode response profile. The radiance desired for the calibration analysis is, however, the incident radiance weighted by the camera response profile S_λ. We obtain these by again assuming a model for the relative spectral shape of the input. That is, the product $L_b N_\lambda$ provides an estimate of the camera-incident spectral radiance

$$\mathcal{L}^{\text{std}} = \frac{\int L_\lambda S_\lambda \lambda\, d\lambda}{\int S_\lambda \lambda\, d\lambda} = \frac{\int L_b N_\lambda S_\lambda \lambda\, d\lambda}{\int S_\lambda \lambda\, d\lambda}. \tag{4}$$

That is, in combining (3) and (4), we have measured the sphere radiance with the photodiode standards, then made a slight correction for the differences in the photodiode-to-camera spectral response profile differences. Note that our convention is to use script notation to denote a variable that is band-weighted, such as $\mathcal{L}^{\text{std}}$, and therefore dependent on the camera properties. Plain characters are used to denote a parameter reported at one specific wavelength, such as the sphere spectral output L_λ or L_b. The standardized spectral response profile S_λ used in this equation is known at both in- and out-of-band wavelengths. As was discussed in the previous section, it is created from an average over all the measured values R_λ.

Fig. 5 depicts the radiometric calibration setup. The aperture of the integrating sphere is sized and positioned to overfill the field-of-view of each camera. This simulates the earth-view geometry and allows inclusion of stray and scattered light sources. The sphere is 1.6 m (65″) in diameter, has a 76 × 23 cm (30 × 9″) exit port, and a 30-cm (12″) external sphere with variable aperture. It is sequenced through a number of lamp-on settings, allowing digital data to be collected at 12 radiometric levels, evenly spaced within the dynamic range of each spectral channel. Operationally, the sphere is initially turned on to its maximum intensity setting and allowed to warm up for 20 min. After data acquisition at this level, the remaining output levels are achieved more quickly in that all bulb transitions are from on to off. This full-on-to-lowest output level cycle is repeated three times, to guarantee that the needed data are acquired and as a consistency check. The sphere is calibrated by using the standards at each of its preprogrammed output levels. This is done prior to each camera calibration. The standards view the sphere through the vacuum chamber window, as this is the viewing configuration of the cameras during calibration.

The data used to deduce the gain coefficients are those collected with the camera operating in its nominal temperature and integration time configuration: the CCD is stabilized to $-5\ ^\circ$C, the optical bench at $5\ ^\circ$C, and the camera electronics at $10\ ^\circ$C. Data have additionally been collected at the optical bench and camera electronics temperature extremes. The radiometric calibration has been shown to be insensitive to these conditions, as was expected. Additionally, data were acquired at integration times set to half of the on-orbit values. These were used to verify the response with the integration time model for the cameras.

With these data, the coefficients in the calibration equation can be determined for each pixel of each spectral band. This is done, for MISR, using a quadratic calibration equation. This functional form has been shown to produce lower residuals, significant at the lower end of the detector's response range.

TABLE I
CHANNEL AVERAGED GAIN RESPONSE (W m$^{-1}\mu$m^{-1}sr^{-1}/DN). CAMERAS ARE DESIGNATED FROM A THROUGH D, SPANNING A RANGE OF VIEW ANGLES FROM NADIR TO 70.5° FORWARD (f) AND AFTWARD (a) OF NADIR (n)

Camera	G_1			
	Band 1 / Blue	Band 2 / Green	Band 3 / Red	Band 4 / NIR
Df	23.7	23.5	28.1	44.1
Cf	23.2	24.1	29.5	45.0
Bf	23.7	22.6	29.5	45.7
Af	23.4	23.6	29.3	43.8
An	20.9	21.9	30.2	43.7
Aa	23.2	24.3	28.9	42.7
Ba	26.1	23.8	27.5	47.9
Ca	23.0	23.1	27.9	44.7
Da	23.1	22.8	27.5	42.4

The relationship used, in both calibration and Level 1 radiance retrieval, is

$$G_2(\mathcal{L}^{\mathrm{std}})^2 + G_1\mathcal{L}^{\mathrm{std}} + G_0 = \mathrm{DN} - \mathrm{DN}_o \qquad (5)$$

where

$\mathcal{L}^{\mathrm{std}}$	incident radiance, weighted by S_λ, the band-specific standardized response profile [W m^{-2}sr^{-1} μm^{-1}];
DN	camera digital number;
G_2, G_1, and G_0	best fit parameters to the measured radiative transfer curve; and
DN$_o$	digital number associated with the video offset voltage, unique for each line of data, and measured by the overclock pixels for that line.

It has been determined that, for the MISR cameras, the CCD response is nearly linear and the coefficients G_0 and G_2 are small [G_o typically ranges from -5 to 10 DN; G_2 is typically 0.001 DN/(W m^{-2}sr^{-1} μm^{-1})^2]. Inclusion of these terms improves the radiance retrieval at the lowest end of the detector transfer curve. The camera response, therefore, is to first order provided by the G_1 coefficient. A convenient way to summarize this large number of coefficients is by using the gain responses (G_1) averaged over all pixels in each channel, as shown in Table I.

The response variation across the arrays can be depicted by the saturation limits, given in Fig. 6. (The data in this figure are in camera pixel order). These have been computed at nine field points, shown by the symbols, and estimated by interpolation at other field locations. Not shown are the pixel-to-pixel differences, which vary by less than 1% locally. (These per pixel response data have been published in [18].) The saturation limit is defined here as the minimum scene equivalent reflectance that saturates a given detector element. This limit is roughly inversely proportional to the G_1 coefficient. For all but some Band 4 channels at the edge-of-field, there is a large margin between an equivalent reflectance of unity $\rho_{eq} = 1$ and the saturation limit. As the camera analog-to-digital converter reaches saturation before the CCD

full-well capacity is met, there is no response roll-off of the sensor as the saturation limit is approached.

The term "equivalent reflectance," denoted ρ_{eq}, was introduced in the above to indicate an illumination level. As all channels are specified to have the same dynamic range, when reported in equivalent reflectance, and as this parameter has a more intuitive relationship to scene brightness, it is a useful description. The equivalent reflectance is defined as

$$\rho_{eq} = (\pi\mathcal{L}_\lambda)/\mathcal{E}_{0\lambda} \qquad (6)$$

where $\mathcal{L}_\lambda$ is the band-weighted spectral radiance incident at the camera while observing a given target and $\mathcal{E}_{o\lambda}$ is the band-weighted exo-atmospheric solar irradiance at wavelength λ. Throughout this paper, the usage of the term equivalent reflectance is used to refer to a specific incident radiance value.

C. Radiometric Uncertainties

The uncertainties in the radiometric calibration are given in [20]. The absolute radiometric uncertainty is dependent on the accuracy of the laboratory standards, which is estimated to be 0.8%. The uncertainty in filter transmittance is the largest component error at 0.5%. The relative camera-to-camera uncertainty is limited by the temporal stability of the integrating sphere from time of sphere calibration to camera calibration. The sphere is known to be stable to better than 0.3% after the first hour of warm-up and returns to the same output level to within 1% following bulb sequencing. (A temperature stabilized, filtered stability monitor, had it existed, would have reduced the uncertainty in calibration due to sphere fluctuations.) The complete error analysis has demonstrated that MISR has met its radiometric calibration requirements for the preflight phase of the program. A single exception is the camera-to-camera relative uncertainty at full scale. (This calibration will be improved on-orbit, as the instrument simultaneously views common targets, such as the diffuse panels.) For full-scale illumination at a 1σ confidence level, these requirements include an uncertainty in the absolute calibration to within 3%, an uncertainty in camera-relative and band-relative calibrations to within 1%, and an uncertainty in pixel-relative calibration to within 0.5%.

D. Radiometric Model

The MISR team has maintained a radiometric model of the instrument from its early design stages. The earlier model was used to develop the system and component specifications, such as detector quantum efficiency, filter transmittance, and optical lens properties. It has been used to develop a stray-light model of the instrument, which was in turn used to interpret measured results. Currently, the model is used to predict on-orbit performance. That is, the instrument model has been updated with preflight radiometric and spectral calibration results, then used to predict saturation limits and SNR for the solar-illuminated scenes to be measured during the mission.

With the radiometric model, the response of the MISR line arrays is given as a function of the integration time t and
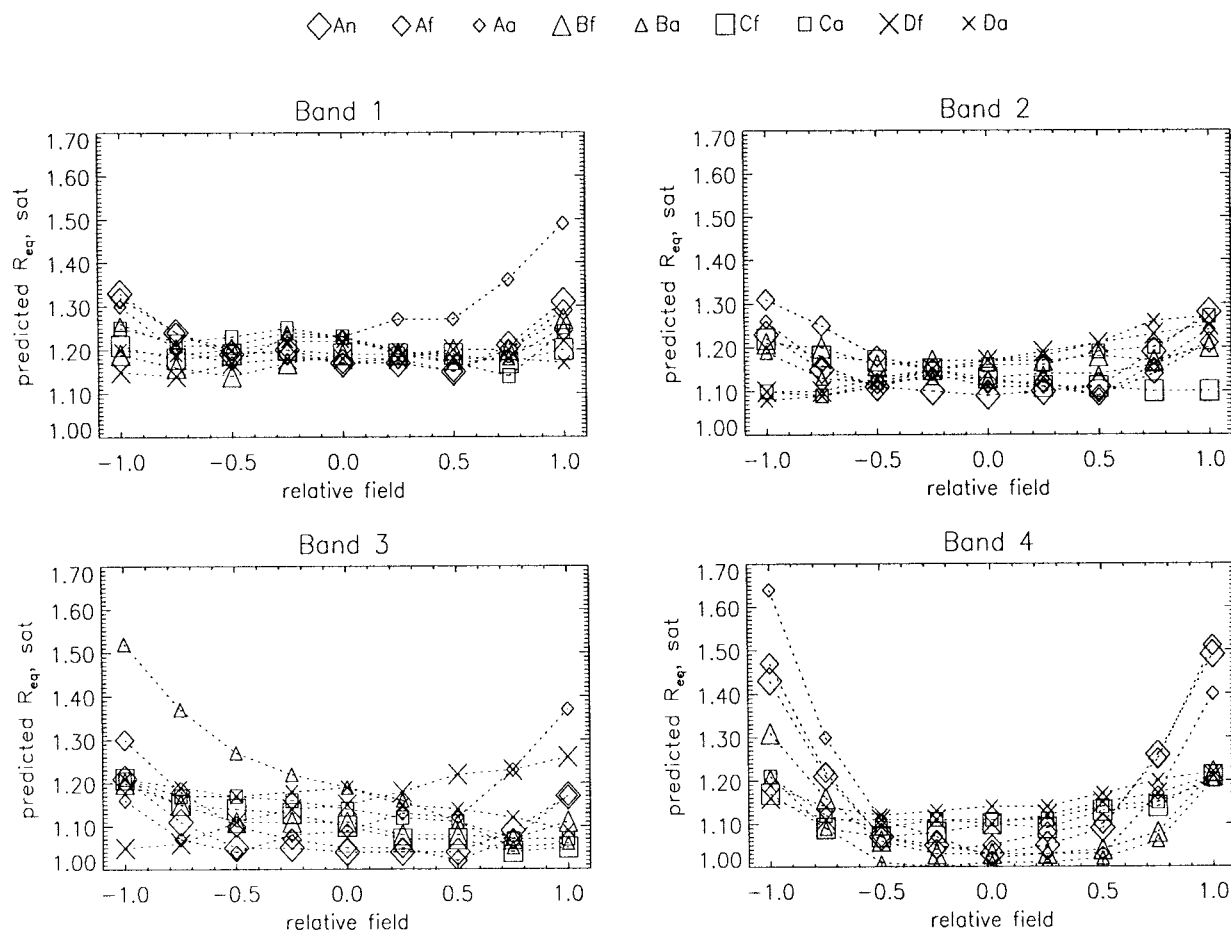
Fig. 6. Saturation values per channel and field angle.

analog-to-digital conversion factor g[DN/electron]. That is

$$G_1^{\text{model}} = \frac{A\Omega tg}{hc} \int_{365}^{1100} R_\lambda \lambda \, d\lambda \qquad (7)$$

where the camera response function R_λ includes the detector quantum efficiency and any optical transmittance terms, including the filter and lens.

One application of the radiometric model, to combine the in-band and out-of-band spectral response profiles, is detailed here. Prior to the spectral calibration of a camera, a combined radiometric and spectral model for that camera is prepared. This model combines component spectral measurements, which are scaled to absolute transmittance by the system-level radiometric calibration. It therefore is an estimate of the measured spectral response profile of each channel, but is provided on an absolute transmittance scale. These models are then used to adjust the measured spectral data to an absolute scale. It is these scaled spectral data that are reported to the ARP.

The lower wavelength cut off of the model (365 nm) has been determined using the Code V lens design program. This code contains the MISR lens model and includes a database giving spectral transmittance of the lens and antireflection coatings. This model has been verified by comparing the predicted transmittances to measured test pieces for the entire

365–1100-nm spectral range. The upper cut off of the cameras (1100 nm) is provided by the band-gap of the silicon detectors. This model predicts a cut off of 1107 nm at 25 °C. In fact, the extrapolated measured transmittance predicts that the spectral response goes to 10^{-6} at 1050 nm.

The following are used as input to construct the complete model.

- *Lens data file*: contains lens transmittance, including the detector window and projected solid angle as a function of wavelength and relative field positions 0.0, 0.25, 0.5, 0.75, and 1.0. Symmetry in the cross-track field is assumed, and data are assumed to be uniform in the much narrower downtrack field. These data are based on the CODE V model.
- *Focal plane data file*: contains spectral quantum efficiency of the filtered detector used in the current camera produced from Sensor Test Set measurements (data are assumed to be pixel invariant). Measurement range is 350–1000 nm. Linear extrapolation is used for wavelengths outside this range.
- *Flat-field file for each channel*: contains offset subtracted data numbers averaged over 100 pixel blocks that map to the relative field positions 0.0, +0.25, ±0.5, ±0.75, and ±1.0 and the applicable offset for each channel. This is

the measured response of the camera to the integrating sphere.

- *Detector gains (electrons/DN)*: for each channel, as measured by the camera light transfer test.
- *Integration times*: used for each channel at which the flat-field data files were acquired.
- *Radiance of the sphere*: output for each channel corresponding to the flat-field files.

With these inputs, a predicted signal in DN is derived based on the unmodified model parameters and input conditions. The integrating sphere is modeled as a 3100-K blackbody, and the blackbody curve is scaled so that the radiance at the band-center wavelength matches the calibrated sphere radiance for the channel and flat-field file. Next, a comparison is made to the actual measured signal in the flat-field files. A scale factor is determined as the ratio of measured-to-predicted signal. The model response is then adjusted by the scale factor to arrive at the adjusted spectral response model. A separate scale factor is computed at each of the nine field positions for a given channel. The scale factor is assumed to be spectrally flat for the channel and field position to which it is applied.

Following acquisition of the flat-field radiance file, there is an opportunity to compare the component-based radiometric model to the as-built system-response measurements. The scale factors, averaged for the nine MISR cameras, were 77, 89, 87, and 87%, respectively, for Bands 1–4. Thus, the component model is shown to be 15% accurate, on average.

E. SNR

Another important system characterization is that of SNR. This is done for each pixel and as a function of illumination level using data acquired for radiometric calibration analysis. During preflight testing, there were 64 repetitions of data N, taken at each illumination level. Following this time series of data acquisitions, the SNR is computed as the average of the offset subtracted DN values to their standard deviation

$$\overline{DN} = \frac{1}{N} \sum_{i=1,N} (DN_i - DN_o) \tag{8}$$

$$SNR^{meas} = \frac{\overline{DN}}{\left(\sqrt{\frac{1}{N-1} \sum_{i=1,N} [(DN_i - DN_o) - \overline{DN}]^2} \right)}. \tag{9}$$

As the MISR team has defined the signal to be that attributed to an in-band response, this measured SNR needs to be multiplied by the ratio of the in-band-to-total-band signal. This ratio is near unity, and no correction was made for the purpose of providing the preflight specification verifications. (Subsequent reporting of measured SNR, using data acquired on-orbit, will include this adjustment.) Following data acquisition and analysis, all cameras were verified to pass their SNR performance

specifications by a large margin. The measured SNR was found to be 986 on average, for full-scale illumination, far exceeding the requirement of 700. The cameras have excellent SNR properties, and they are photon-noise limited for signals greater than 1% in equivalent reflectance [20].

In addition to this measure of SNR, the radiometric model is used to predict on-orbit SNR. We would not necessarily expect these results to be the same, as the source spectra in the laboratory (tungsten bulbs) differ from the on-orbit calibration source (a diffuse panel that is solar illuminated). For the model, first the in-band signal is computed

$$Sig^{in\text{-}band} = \frac{A\Omega t}{hc} \int_{0.365}^{1.1} E_{o\lambda} \rho_{eq} S_\lambda^{in\text{-}band} \lambda \, d\lambda. \tag{10}$$

The noise is computed as the root-sum-square of the photon noise, quantization noise, and other electronic noise. The photon noise, in turn, is computed as a function of the total signal plus a contribution due to dark current i_{dark}

$$N_p = \sqrt{Sig^{total\text{-}band} + i_{dark} t} \tag{11}$$

whereas the quantization noise, for this case, a 14-bit linear digitalization and 12-bit square-root encoding, is given by (12) (with FW being the full-well capacity in electrons), shown at the bottom of the page, and the electronic noise is estimated to be 55 electrons.

Combining these, we obtain

$$SNR = \frac{Sig^{in\text{-}band}}{\sqrt{N_p^2 + N_q^2 + N_o^2}}. \tag{13}$$

For the case in which onboard pixel averaging is enabled, the SNR is expected to increase, as the photon and other noise is reduced by the square-root of the number of pixels averaged. From this model, we believe that the SNR specifications will be met on-orbit for all averaging configurations specified for the instrument.

IV. GEOMETRIC CALIBRATION

A. Camera Pointing Determination

To be of value to the scientific community, MISR's 36 independent data channels must be coregistered. This will be accomplished on-orbit by the use of navigation and attitude data from the spacecraft as well as a camera pointing model. This model is established preflight and updated as needed on-orbit. For the preflight determination, an instrument termed the Collimator Array Tool (CAT) has been used (pictured in [21]). The CAT, designed and manufactured at JPL, consists of nine small collimators, each of which projects a target into the MISR camera at the nominal angles. The CAT registers to three tooling points on the MISR optical bench so as

$$N_q = \sqrt{\left(\frac{FW}{\sqrt{12} \cdot 2^{(14-1)}}\right)^2 + \frac{2\sqrt{FW \cdot (Sig^{total\text{-}band} + i_d \cdot t + DN_o/g)}}{\sqrt{12} \cdot 2^{12}}} \tag{12}$$

<div align="center">

TABLE II
CAMERA POINTING SUMMARY
</div>

Camera	Specified camera pointing angles and tolerances		As-built versus specified pointing angle difference	
	Boresight Angle (β) ($\pm 0.2°$)	Offset Angle (δ) ($\pm 0.2°$)	Boresight Angle (β)	Offset Angle (δ)
Df	+58.0°	-2.7°	-0.12°	-0.10°
Cf	+51.2°	-2.3°	0.03°	-0.09°
Bf	+40.0°	-1.7°	0.03°	0.00°
Af	+23.3°	-1.0°	-0.01°	0.07°
An	0.0°	0.0°	-0.01°	0.01°
Aa	-23.3°	+1.0°	-0.01°	-0.07°
Ba	-40.0°	+1.7°	-0.02°	-0.06°
Ca	-51.2°	+2.3°	-0.07°	0.09°
Da	-58.0°	+2.7°	-0.01°	0.03°

to provide precise repeatability and thermal isolation. The nine collimator targets are illuminated using three quartz-tungsten sources and fiber-optic cables. Each collimator target is adjusted to be within 20 arcsec of the nominal camera angles. A table of deviation permits further refinement. A small integrating sphere resides within the dome cap on the target assembly. This configuration is used to provide uniform illumination of the target.

The target that is projected into each camera consists of 21 illuminated lines. By evaluation of the target projection onto the focal plane, the camera pointing and rotation angles are determined. Results of CAT testing are given in Table II and have indicated 1) that the MISR cameras have been built to their design angles, to within their allowed tolerances, 2) the cameras alignments are such as to provide the required swath overlap of all 36 channels, and 3) the boresight shifts were insignificant following vibrational testing of the instrument.

B. Distortion Mapping

The cross-track pixel pointing angle relative to the camera boresight is one of the parameters that is expected not to change from its ground measurements. This eliminates one set of variables in the camera model, reducing the number of parameters that must be varied to match the results of ground control point measurements. In order to fully take advantage of this inflight pointing calibration, the cross-track pointing angle should be known with the same, or better, accuracy as the ground control point image. Hence, the goal of the laboratory pixel cross-track pointing measurements was set at 1/8 pixel. The entire error budget for pixel registration is 0.5 pixel.

The cross-track pixel pointing angle has been determined, for each channel, through a measure of the image distortion. This is the deviation in field angle for the illumination of a given pixel, as compared to the geometrically derived field angle

$$\text{distortion} = \theta - \omega. \qquad (14)$$

Here θ is the incident field angle. The angle ω is computed as the inverse tangent of x divided by the effective focal length (EFL) of the camera, where x is the distance from the image centroid distance to the boresight center. Distortion is only measured in the cross-track direction. The design shows that the distortion is negligible in the downtrack direction, as the

downtrack angle is only 2% of the extent of the cross-track field-of-view.

The key to acquiring these data was a test setup, where a pinhole object of a known field angle could be imaged onto the camera focal plane. The facility assembled to perform distortion mapping is called the Optical Characterization Chamber (OCC). A xenon lamp source external to this chamber feeds a chamber-internal target wheel. At the target wheel, a pinhole is selected according to the focal length of the camera under test. The source is spectrally filtered to match the in-band color of the array being illuminated. The pinhole target is at the focus of a collimator, allowing the camera to image the pinhole, which produces a subpixel Airy disk when well focused. The camera is attached to a two-axis gimbal, and this pinhole image can be scanned across the focal plane in either the downtrack or cross-track directions. After data acquisition, the data are fitted to a fifth-order polynomial, giving the tangent of the field angle as a function of pixel number. The fit of the data to the polynomial verified to be between 1/10 and 1/20 of a pixel. Such a plot is shown in Fig. 7, for the An camera, Red Band. The distortion was measured at 0, 5, and 10 °C and found to be small (less than a pixel for most field points) and relatively insensitive to temperature.

In addition to distortion, the OCC facility was used to measure boresight pixel (defined here as the pixel that is illuminated when the field angle is perpendicular to the camera head flange), modulation transfer function (MTF), point-spread function (PSF), and the EFL of the camera under test.

C. PSF

The 3% absolute radiometric requirement (1σ at foil scale) specified for MISR applies to the accuracy of measuring radiance for a spatially homogeneous target. MISR additionally has specifications for radiometric accuracy over targets that have contrast variations across the swath. The specifications are that there must be no more than a 2% radiometric error when radiance is measured over each of two targets. The first case considers radiance at 8 pixels-distance from an ocean-cloud boundary (specified as a scene composed of two half-planes of 5 and 100% reflectance, respectively); the second case considers radiance in the center of a 24 × 24 pixel lake, placed in the middle of a land target (specified as a scene with a background reflectance of 50% and lake reflectance of 5%).

In verifying this specification, it was decided that the cameras PSF (response to a point source object) would be measured. The PSF could then be convolved with the targets to be verified, to see if blurring is sufficient to reduce the radiometric accuracy. Following this procedure, it was determined that the radiometry for the ocean-cloud target was accurate, but that the specification was not met for the lake scene. As a consequence of this study, the measured PSF data have been made available within the ARP and will be used to provide image contrast enhancement to the MISR data as part of the standard processing.

The PSF was measured by using the OCC facility described above. The image of a pinhole object was made to illuminate
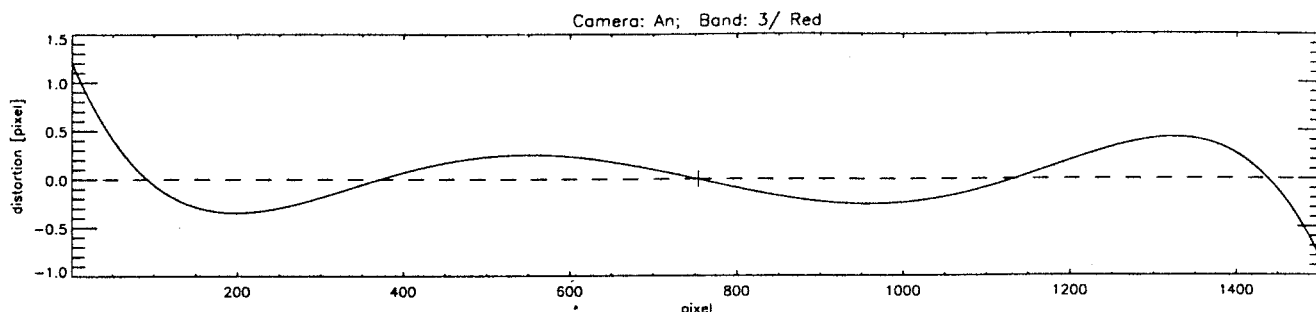
Camera: An; Band: 3/ Red

Fig. 7. Distortion map for the An camera, Red Band.

TABLE III
PERFORMANCE TESTING SUMMARY

Parameter	Specification	Performance
Modulation Transfer Function (MTF)	0.24 at 23.8 cycles per mm, beginning of life	Pass.
Effective focal length (EFL)	59.3 (A) 73.4 (B) . 95.3 (C) . 123.8 (D) mm.	58.90 (Af), 58.90 (An), 59.03 (Aa) 73.02 (Bf), 73.00 (Ba) 95.34 (Cf), 95.32 (Ca) 123.67 (Df), 123.65 (Da) Pass. These values are within the manufacture tolerance specification.
Saturation blooming	Radiometric effects negligible eight pixels distance from saturated pixel.	Failed. Saturation blooming evident some 30 pixels away from the saturated pixel.
Local uniformity	3% standard deviation among consecutive four pixels	Majority pass with <1% deviation. Nine pixel sets have >10% response deviation, out of 13,000 possible sets.
Polarization insensitivity	± 1%	Pass. Lyot depolarizer/ gaussian filter combination effective.

the detector array. This image was scanned across the array by rotating the gimbal on which the camera was mounted. The DN's from a given reference pixel were recorded as the pinhole image scanned a total of 51 pixels in distance, along the cross-track direction. This scan was centered about the reference pixel and moved in 1/10 pixel increment steps. The PSF was computed by averaging all ten DN values recorded, while the illuminated region fell within each of the 51 pixels in turn. The results were then normalized to have an area of unity value. The PSF results, shown in Fig. 8, have a half width several pixels across. The observed PSF was larger than that predicted from physical optics (i.e., the Airy disk predicted from diffraction). This has been attributed to scattering between the focal plane detectors and filter [22].

V. SUMMARY

The primary calibration experiments have been described in the above sections. Additionally, many performance verifications were conducted during preflight testing, as summarized in the Table III. The design was shown to be verified in terms of MTF, EFL, detector response uniformity (among a local collection of pixels), and polarization. Saturation blooming was noted across a line array.

For the generation of MISR data products, a sophisticated data quality assessment algorithm will identify all pixels that are radiometrically affected by saturation or other specification errors. Pixels for which the specifications fail will not be used in science data product generation. Other data quality checks
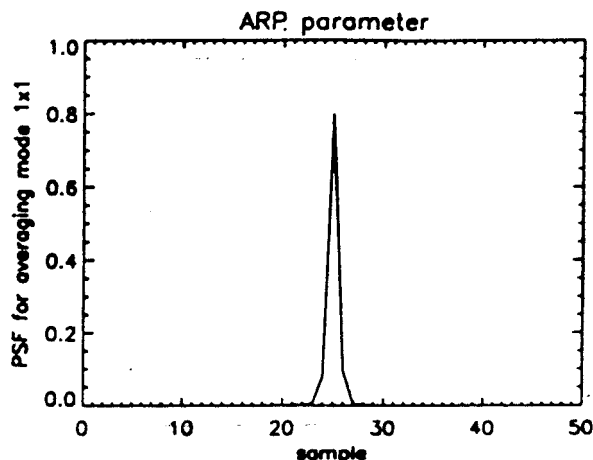

Fig. 8. PSF for the nadir camera (AN), Red Band.

are for detector failures (e.g., poor signal-to-noise) or for pixels which have a low DN when the data line has an atypically high-average DN. The latter is tracked, as at high illumination levels it is noted that there is an uncertainty in the measured video offset, as determined by sampling the overclock pixels. This uncertainty is small ($\sim$25 DN for an average DN of 12 000 for the line) and, therefore, will seldom be problematic.

The MISR cameras have been calibrated and tested to demanding specifications. Care in the development of the test configurations and analysis tools were needed to meet this challenge. Exceptions to the specification verifications are

mostly inconsequential and include a spectrally integrated out-of-band response of 3%, for one spectral channel, in contrast to the challenging requirement of a 1% out-of-band response. Additionally, a finite PSF was measured, attributed to a low level of scattering between each CCD array and its associated spectral filter. This is thought to violate a requirement that states that scattering must be sufficiently low so as to produce accurate radiometry, even for a high contrast scene, such as that of a dark lake surface surrounded by a bright land mass. Although corrections are not needed for most scene types, it is found that the calibration data are of sufficient quality to provide data conditioning, as needed, to correct for the out-of-band response and provide image contrast enhancement. With these tools, MISR is able to meet even its most challenging performance specifications.

ACKNOWLEDGMENT

REFERENCES

[1] D. J. Diner, J. C. Beckert, T. H. Reilly, C. J. Bruegge, J. E. Conel, R. A. Kahn, J. V. Martonchik, T. P. Ackerman, R. Davies, S. A. W. Gerstl, H. R. Gordon, J.-P. Muller, R. B. Myneni, P. J. Sellers, B. Pinty, and M. M. Verstraete, "Multi-angle Imaging SpectroRadiometer (MISR) instrument description and experiment overview," this issue, pp. 1072–1087.

[2] V. M. Jovanovic, M. M. Smyth, J. Zong, R. Ando, and G. W. Bothwell, "MISR photogrammetric data reduction for geophysical retrievals," this issue, pp. 1290–1301.

[3] J. V. Martonchik, D. J. Diner, R. A. Kahn, T. P. Ackerman, M. M. Verstraete, B. Pinty, and H. R. Gordon, "Techniques for the retrieval of aerosol properties over land and ocean using multiangle imaging," this issue, pp. 1212–1227.

[4] J. V. Martonchik, D. J. Diner, B. Pinty, M. M. Verstraete, R. B. Myneni, Y. Knyazikhin, and H. R. Gordon, "Determination of land and ocean reflective, radiative, and biophysical properties using multiangle measurements," this issue, pp. 1266–1281.

[5] C. J. Bruegge, M. L. White, N. L. Chrien, E. B. Villegas, and V. G. Ford, "Multi-angle Imaging SpectroRadiometer (MISR) design issues influenced by performance requirements," in *Proc. SPIE, Sensor Syst. Early Earth Observing Syst. Platforms,* Apr. 1993, vol. SPIE-1939, pp. 104–113.

[6] B. C. Johnson, Y. Barnes, T. R. O'Brian, J. J. Butler, C. J. Bruegge, S. Biggar, P. Spyak, and M. Pavlov, "Initial results of the bidirectional reflectance characterization round-robin in support of EOS AM," in *Conf. Issue: New Develop. Applicat. Opt. Radio. (NEWRAD'97), Metrologia,* to be published.

[7] K. Thome, S. Schiller, J. E. Conel, K. Arai, and S. Tsuchida, "Results of the 1996, joint, EOS vicarious calibration campaign to Lunar Lake, NV," in *Conf. Issue: New Develop. Applicat. Opt. Radio. (NEWRAD'97), Metrologia,* to be published.

[8] C. J. Bruegge and R. M. Woodhouse, *In-Flight Radiometric Calibration and Characterization Plan, JPL D-13315,* Jet Propul. Lab., Pasadena, CA, Apr. 29, 1996.

[9] R. M. Woodhouse, C. J. Bruegge, B. J. Gaitley, C. Saghri, and N. L. Chrien, "Multi-angle Imaging SpectroRadiometer (MISR) ancillary radiometric product (ARP)," in *Proc. SPIE 3117, Earth Observing Syst. 11,* San Diego, CA, July 1997.

[10] C. J. Bruegge, D. J. Diner, and V. G. Duval, "The MISR calibration program," *J. Atmos. Ocean. Tech.,* vol. 13, no. 2, pp. 286–299, 1996.

[11] C. J. Bruegge, V. G. Duval, N. L. Chrien, and D. J. Diner, "Calibration plans for the Multi-angle Imaging SpectroRadiometer (MISR)," *Metrologia,* vol. 30, no. 4, pp. 213–221, 1993.

[12] C. J. Bruegge, V. G. Duval, N. L. Chrien, and R. P. Korechoff, "MISR instrument development and test status," in *Proc. EUROPTO/SPIE, Adv. Next-Generation Satellites,* Paris, France, Sept. 25–28, 1995, vol. 2538, pp. 92–103.

[13] C. J. Bruegge, R. M. Woodhouse, and D. J. Diner, "In-flight radiometric calibration plans for the Earth Observing System Multi-angle Imaging SpectroRadiometer," in *Proc. EEE/IGARSS,* Lincoln, NE, Paper 96.1028, May 27–31, 1996.

[14] E. B. Hochberg, M. L. White, R. P. Korechoff, and C. A. Sepulveda, "Optical testing of MISR lenses and cameras," in *Proc. SPIE, Opt. Spect. Tech. Instrum. Atmos. Space Res. 11* Denver, CO, Aug. 5–9, 1996, vol. 2830.

[15] R. P. Korechoff, D. Kirby, E. Hochberg, C. Sepulveda, and V. Jovanovic, "Distortion calibration of the MISR linear detectors," in *Proc. SPIE, Earth Observing Syst.,* Denver, CO, Aug. 5–9, 1996, vol. 2820.

[16] I. M. Palmer, "Effective bandwidths for Landsat-4 and Landsat-D' multispectral scanner and Thematic Mapper subsystems," *IEEE Trans. Geosci. Remote Sensing,* vol. GE-22, pp. 336–338, May 1984.

[17] C. Wehrli, *Extraterrestrial Solar Spectrum, World Radiation Center (WRC).* Davos-Dorf, Switzerland: WRC, Pub. 615, July 1985,.

[18] C. J. Bruegge, N. L. Chrien, B. J. Gaitley, and R. P. Korechoff, "Preflight performance testing of the Multi-angle Imaging SpectroRadiometer cameras," in *Proc. SPIE 2957, Satellite Remote Sensing 111,* Taormina, Italy, Sept. 23–26, 1996.

[19] N. L. Chrien and C. J. Bruegge, "Out-of-band spectral correction algorithm for the Multi-angle Imaging SpectroRadiometer," in *Proc. SPIE, Earth Observing Syst.,* Denver, CO, Aug. 5–9, 1996, vol. 2820.

[20] C. J. Bruegge, N. L. Chrien, D. J. Diner, R. A. Kahn, and J. V. Martonchik, "MISR radiometric uncertainty analyses and their utilization within geophysical retrievals," in *Conf. Issue: New Develop. Applicat. Opt. Radio. (NEWRAD'97), Metrologia,* to be published.

[21] C. J. Bruegge and D. J. Diner, "Instrument verification tests on the Multi-angle Imaging SpectroRadiometer (MISR)," in *Proc. SPIE 3117, Earth Observing Syst. 11,* San Diego, CA, July 28–29, 1997.

[22] R. P. Korechoff, D. J. Diner, D. J. Preston, and C. J. Bruegge, "Spectroradiometer focal-plane design considerations: Lessons learned from MISR camera testing," in *Proc. EUROPTO/SPIE, Adv. Next-Generation Satellites,* Paris, France, Sept. 25–28, 1995, vol. 2538, pp. 104–106.

Carol J. Bruegge received the B.A. and M.S. degrees in applied physics from the University of California at San Diego in 1978 and the M.S. and Ph.D. degrees in optical sciences from the University of Arizona, Tucson, in 1985.

She has been with the Jet Propulsion Laboratory, California Institute of Technology, Pasadena, since 1985, where she is presently a Member of the Technical Staff. Her experience is principally in the areas of terrestrial remote sensing, radiative transfer, instrument calibration, and the application of ground-truth measurements to the radiometric calibration of remote-sensing instruments, such as the Landsat Thematic Mapper, the Airborne Imaging Spectrometer (AIS), and the Airborne Visible/Infrared Imaging Spectrometer (AVIRIS). She has participated in the First International Land Surface Climatology Program Field Experiment (FIFE) as a Principal Investigator. She is presently the Instrument Scientist for MISR, for which she oversees the preflight and inflight radiometric calibration and characterization efforts and coordinates the activities of the MISR calibration and validation teams.

Valerie G. Duval received the B.A. degree in physics from New Mexico State University, Las Cruces, in 1981.

She has been with the Jet Propulsion Laboratory, California Institute of Technology, Pasadena, since 1981. She has worked on the development of SWIR HgCdTe detector arrays for imaging spectrometer instruments as well as provided system analysis and engineering for imaging spectrometer instrumentation. From 1990 to 1996, she joined the MISR team as a Calibration Engineer. She is currently Supervisor of the Detector and Sensor System Prototyping Group.

Barbara J. Gaitley received the B.A. and M.S. degrees in mathematics from California State University, Northridge.

She is currently with the Jet Propulsion Laboratory, California Institute of Technology, Pasadena, working on data analysis and software development for field instruments used in MISR validation and vicarious calibration. She also processed and summarized MISR camera preflight calibration data. Her research experience includes algorithm development, parameter studies, data analysis, and software development in private industry.

Nadine L. Chrien received the B.S. degree in engineering in the field of systems science from the University of California, Los Angeles, and the M.S. degree in optical sciences from the University of Arizona, Tucson.

She is currently with the Jet Propulsion Laboratory, California Institute of Technology, Pasadena, as a Systems Analyst for MISR and is working as part of the MISR In-Flight Radiometric Calibration and Characterization Team on algorithm development. Prior to her work on MISR, she worked on the Mars Observer Pressure Modulator Infrared Radiometer (PMIRR) alignment, target simulator, and calibration monochromator systems.

Eric B. Hochberg received the B.S. degree in optical engineering from the University of Rochester, Rochester, NY, in 1976.

He was with Xerox Corporation, Rochester, NY, where he worked on many laser, image processing, fiber-optic, and holographic systems. He is currently with the Jet Propulsion Laboratory, California Institute of Technology, Pasadena, working on optical metrologies for testing and characterization of a variety of astronomical and earth remote-sensing instruments. He holds five patents.

Robert P. Korechoff received the B.S., M.S., and Ph.D. degrees in physics from the University of California, Los Angeles.

He was a Member of the Technical Staff at Pacific-Sierra Research Corporation, Santa Monica, CA, and the Hughes Aircraft Company, Culver City, CA. He is currently with the Jet Propulsion Laboratory, California Institute of Technology, Pasadena, as Technical Group Leader in the Space Instruments Implementation Section. He was the Optical Systems Engineer on the second generation Wide Field/Planetary Camera for the Hubble Space Telescope, prior to his work on MISR. Presently, he holds the same position for the Space Interferometry Mission.